1,1'-Disubstituted Ferrocenes as Donors for Charge-Transfer Complexes. Synthesis, Structure, Conductivity, and Magnetic Properties

Antonio Togni,*,† Markus Hobi,† Grety Rihs,‡ Günther Rist,‡ Alberto Albinati,§ Piero Zanello,⊥ Damian Zech,∥ and Hugo Keller∥

Laboratory of Inorganic Chemistry, Swiss Federal Institute of Technology, ETH-Zentrum, CH-8092 Zürich, Switzerland, Central Research Services, CIBA-GEIGY Ltd., K-127, P.O. Box, CH-4002 Basel, Switzerland, Institute of Pharmaceutical Chemistry, University of Milan, I-20131, Italy, Department of Chemistry, University of Siena, Pian dei Mantellini, 44, I-53100 Siena, Italy, and Physics Institute, University of Zürich, Winterthurerstrasse 190, CH-8057 Zürich, Switzerland

Received October 29, 1993®

Starting from ferrocene-1,1'-dicarbaldehyde (1), the novel electron donors 1,1'-bis[(5,6-dihydro-1,3-dithiolo[4,5-*b*][1,4]dithiin-2-ylidene)methyl]ferrocene (**5**), 1,1'-bis[(1,3-benzodithiol-2-ylidene)methyl]ferrocene (**6**), and 1,1'-bis[2-[4-(methylthio)phenyl]-(*E*)-ethenyl]ferrocene (**7**) were prepared, and their electrochemical properties were studied. **5** and **6** undergo two reversible oxidation processes, whereas for **7** only the first electron removal is reversible in character. Crystals of **5** are monoclinic, space group $P2_1/c$, with a = 12.448(1) Å, b = 12.178(1) Å, c = 16.219(1) Å, β = 104.5(1)°, and Z = 4. In the solid state, molecules of **5** assume an eclipsed conformation, with the two substituents lying on top of each other (*intramolecular stacking*). **5** and **6** easily form 1:2 electron-transfer complexes with TCNQ (**8** and **9**, respectively), whereas **7** leads to a charge-transfer (CT) complex (**10**). Polycrystalline samples of **8** and **9** are conducting: σ_{rt}(**8**) = 0.26 S·cm^{-1} and σ_{rt}(**9**) = 0.20 S·cm^{-1}. SQUID magnetic susceptibility measurements of **8** and **9** show these materials to undergo a phase transition dominated by a weak antiferromagnetic coupling (Curie–Weiss constants θ (**8**) = −3 K and θ (**9**) = −3 K). **10** is an insulator and is characterized by a very weak degree of electron transfer. Crystals of **10** are triclinic, space group $P\bar{1}$, with a = 7.796(1) Å, b = 8.607(1) Å, c = 16.396(2) Å, α = 92.88(1)°, β = 97.83(1)°, γ = 100.95(1)°, and Z = 1. In the CT complex **10**, the donor **7** assumes an antiperiplanar conformation, thus leading to a 1D-DADA type structure.

Introduction

After the discovery of organic superconducting charge-transfer (CT) complexes,[1] the interest in this field has grown steadily.[2] The key organic electron donors are related to tetrathiafulvalene (TTF), and structural variations of this prototype have been carried out extensively, but organometallic compounds as partners for the formation of such CT complexes have received little attention, as far as electrically conducting materials are concerned.[3] On the other hand, the magnetic properties of CT complexes of peralkylated ferrocenes (and other metallocenes) have been intensively studied by Miller and coworkers and have lead to the discovery of the first organometallic bulk ferromagnet, [FeCp*2][TCNE].[4] In these cases, the importance of the highly symmetric permethylated ferrocene has been stressed as one of the factors allowing for cooperative magnetic coupling, thus being responsible for the properties of these materials.[5]

We report herein the facile synthesis of novel ferrocene derivatives bearing just two conjugated substituents in the 1,1'-position and their incorporation into CT complexes, the structural, electric, and magnetic properties of which depend on the nature of the substituents. The underlying idea is to create extended electron-donor systems containing fragments capable of *intramolecular* stacking, by virtue of the eclipsed conformation of the ferrocene moiety. This conformation should be favored over other possible ones, if the two fragments attached to the ferrocene are able of undergoing attractive interactions with one another, and should lead to structures containing separate stacks of donors and acceptors, respectively, thus affording conductive materials. On the other hand, if the preferred conformation is such that the two substituents

† Swiss Federal Institute of Technology.
‡ CIBA-GEIGY Ltd.
§ University of Milan.
⊥ University of Siena.
∥ University of Zürich.

® Abstract published in *Advance ACS Abstracts,* March 1, 1994.

(1) (a) Jérome, D.; Mazaud, A.; Ribault, M.; Bechgaard, K. *J. Phys. Lett (Paris)* **1980**, *41*, L95-L98. (b) Bechgaard, K.; Jacobsen, C. S.; Mortensen, K.; Pedersen, M. J.; Thorup, N. *Solid State Commun.* **1980**, *33*, 1119–1125. (c) Bechgaard, K.; Carneiro, K.; Rasmussen, F. G.; Olsen, K.; Rindorf, G.; Jacobsen, C. S.; Pederson, H. J.; Scott, J. E. *J. Am. Chem. Soc.* **1981**, *103*, 2440–2442.

(2) For reviews, see, e.g.: (a) Williams, J. M.; Ferraro, J. R.; Thorn, R. J.; Carlson, K. D.; Geiser, U.; Wang, H. H.; Kini, A. M.; Whangbo, M.-H. *Organic Superconductors, Synthesis, Structure, Properties, and Theory*; Prentice Hall: Englewood Cliffs, NJ, 1992. (b) Bryce, M. R. *Chem. Soc. Rev.* **1991**, *20*, 355–390. (c) Graja, A. *Low-Dimensional Organic Conductors*; World Scientific: Singapore, 1992.

(3) For isolated reports on conducting properties of ferrocene-containing CT complexes, see, e.g.: (a) Müller-Westerhoff, U. T.; Eilbracht, P. *J. Am. Chem. Soc.* **1972**, *94*, 9272–9274. (b) Matsubayashi, G.; Yokozawa, A. *Inorg. Chim. Acta* **1992**, *193*, 137–141.

(4) (a) Miller, J. S.; Calabrese, J.; Rommelmann, H.; Chittipeddi, S. R.; Zhang, J. H.; Reiff, W. M.; Epstein, A. J. *J. Am. Chem. Soc.* **1987**, *109*, 769–781. (b) For a recent review on the magnetic properties of metallocenium-based electron-transfer salts, see: Miller, J. S.; Epstein, A. J. In *Research Frontiers in Magnetochemistry*; O'Connor, C. J., Ed.; World Scientific: Singapore, 1993; pp 283–302.

(5) See, e.g.: (a) Miller, J. S.; Epstein, A. J. In *Magnetic Molecular Materials*; Gatteschi, D., Kahn, O., Miller, J. S., Palacio, F., Eds.; NATO ASI Series, Series E: Applied Sciences; Kluwer Academic Publishers: Dordrecht, 1991; Vol. 198, pp 151–158. (b) Miller, J. S.; Epstein, A. J.; Reiff, W. M. *Chem. Rev.* **1988**, *88*, 201–220.

0276-7333/94/2313-1224$04.50/0

Scheme 1

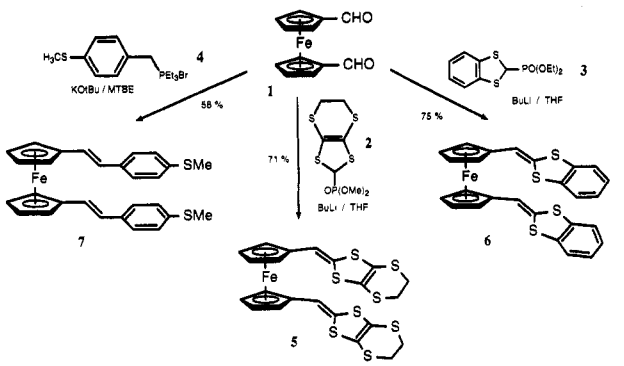

are in an antiparallel arrangement, the corresponding CT complexes with suitable acceptors should give insulating materials, by virtue of an alternation between donors and acceptors, thus possibly giving rise to cooperative magnetic phenomena. Another feature of these compounds is the possibility that they form reversible multistage redox systems, thus, in principle, allowing the alternative incorporation of mono-, di-, and possibly polyradicals of the same basic structure into different magnetic materials.

Results and Discussion

Synthesis of Donors. The donors are easily accessible in one step from ferrocene dicarbaldehyde (**1**)[6] and the appropriate Wittig or Wittig–Horner reagent. The compounds so far studied are illustrated in Scheme 1.

Whereas for the synthesis of compounds **5** and **6** the known phosphonate reagents **2**[7] and **3**[8] could be used, the preparation of derivative **7** was achieved by using the Wittig reagent obtained from **4**, i.e., (4-(methylthio)-benzyl)triethylphosphonium bromide, by deprotonation with KO^{t}Bu in MTBE. These conditions were found to ensure good *E,E*-selectivity, with other Wittig reagents affording much higher amounts of the *Z,E*- and *Z,Z*-isomers. The products were obtained in moderate to good yields as red crystalline materials, which were purified by column chromatography.

Synthesis of CT Complexes and Electrical Conductivity. Compounds **5–7** were found to readily form CT complexes with the classic organic acceptor TCNQ. Typically, the two components were separately dissolved in equal volumes of hot 1,2-dichloroethane and the solutions mixed and briefly stirred. Thereafter, the dark brown solution was allowed to slowly cool to room temperature, whereby needle-like microcrystals of the corresponding CT complexes deposited. These were isolated in 63–86% yield. In all experiments carried out, only black, microcrystalline materials containing the donor and the acceptor in a 1:2 ratio were obtained. This was the case even when TCNQ was used in a substoichiometric amount.

The CT complexes thus obtained (**8–10**) were subjected, in the form of polycrystalline pressed pellets, to measurements of the electrical conductivity at room temperature by the four-probe method. The results obtained

Scheme 2. CT Complexes and Their Room Temperature Conductivity (Pressed Pellets)

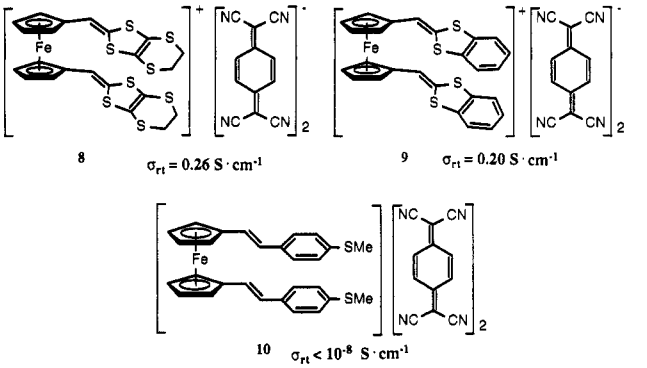

(average of at least two measurements with material from different batches) are indicated in Scheme 2. Whereas complexes **8** and **9** show a substantial conductivity (σ = 0.26 and 0.20 S·cm^{-1}, respectively), derivative **10** is essentially an insulator ($\sigma < 10^{-8}$). Obviously, fundamental structural differences must exist between the two types of CT complexes prepared. A hint as to this is given by the IR spectra of these three derivatives. Compounds **8** and **9** show a strong ν_{CN} band at 2195 and 2200 cm^{-1}, respectively, indicative of the presence of partially reduced TCNQ ([(TCNQ)$_2$]$^-$).[9] The ν_{CN} band for complex **10** is shifted to 2215 cm^{-1} (for comparison, this stretch in TCNQ is observed at 2220 cm^{-1}), indicating that in this complex only weak charge-transfer interactions are present. The relatively high conductivity measured for **8** and **9** suggests that in these two compounds separate stacks of **5**/**6** and TCNQ must be present. Unfortunately, it has not yet been possible to grow single crystals suitable for X-ray diffraction.

Electrochemical Properties. Figure 1a,b shows the cyclic voltammetric responses exhibited by **6** in dichloromethane solution. Three subsequent oxidation processes are displayed, only the first two exhibiting features of chemical reversibility. Controlled potential coulometry in correspondence to the first anodic step (E_w = +0.4 V) consumes one electron/molecule; the originally orange solution assumes a bottle-green color (γ_{max} = 625 nm; ϵ = 3241 M^{-1} cm^{-1}) typical of ferrocenium species, showing a cyclic voltammetric response quite complementary to the first step illustrated in Figure 1a. The second oxidation step, although displaying a good extent of chemical reversibility in cyclic voltammetry and consuming one electron/molecule (E_w = +0.9 V), affords a dirty green solution which no longer exhibits a cyclic voltammetric profile attributable to the generation of redox congeners of **6**. As a matter of fact, exhaustive back-reduction (E_w = 0.0 V) consumes only one electron/molecule and produces a brown solution which gives rise to ill-defined redox processes. This proves that the primarily electrogenerated dication [**6**]$^{2+}$ is a transient species. Finally, the third anodic process is irreversible in character. This third anodic step is thought to be substituent centered, as indicated by the model compound **11** (see Scheme 3) which gives rise to an irreversible oxidation at high-potential values (E_p = +0.93 V).

In this picture it seems reasonable to assign the second anodic step to a ferrocene-based electron removal, too.

(6) Balavoine, G. G. A.; Dosneau, G.; Fillebeen-Khan, T. *J. Organomet. Chem.* **1991**, *412*, 381–382.

(7) (a) Moore, A. J.; Bryce, M. R. *Synthesis* **1991**, 26–28. (b) Varma, K. S.; Bury, A.; Harris, N. J.; Underhill, E. *Syntheis* **1987**, 837–838. (c) Steimecke, G.; Sieler, H.-J.; Kirmse, R.; Hoyer, E. *Phosphorus Sulfur* **1979**, *7*, 49–55.

(8) Akiba, K.; Ishikawa, K.; Inamoto, N. *Bull. Chem. Soc. Jpn.* **1978**, *51*, 2674–2683.

(9) See, e.g.: (a) Ward, M. D.; Johnson, D. C. *Inorg. Chem.* **1987**, *26*, 4213–4227. (b) Miller, J. S.; Zhang, J. H.; Reiff, W. M.; Dixon, D. A.; Preston, L. D.; Reis, A. H., Jr.; Gebert, E.; Extine, M.; Troup, J.; Epstein, A. J.; Ward, M. D. *J. Phys. Chem.* **1987**, *91*, 4344–4360.

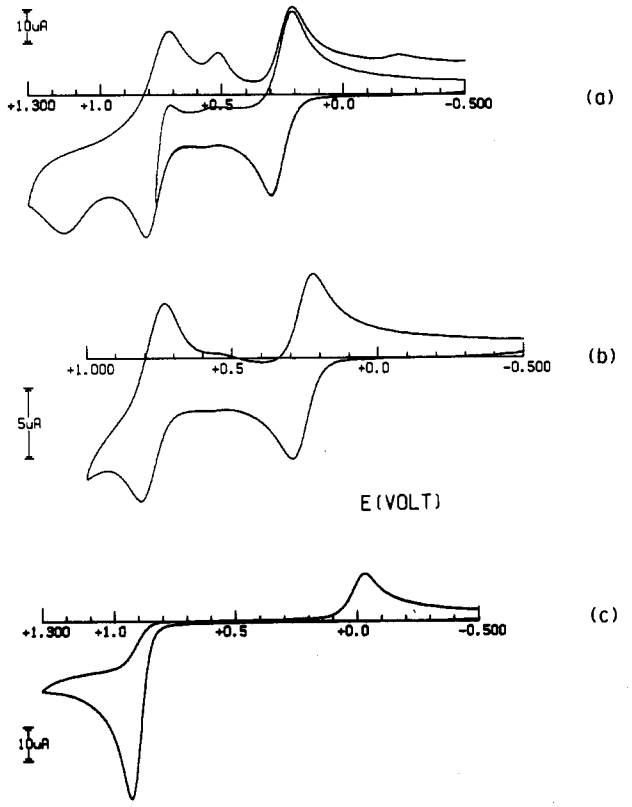

Figure 1. Cyclic voltammograms recorded at a platinum electrode on a CH_2Cl_2 solution containing $[NBu_4][ClO_4]$ (0.2 mol dm^{-3}) and (a, b) **6** (1.0×10^{-3} mol dm^{-3}); (c) **11** (3.5×10^{-3} mol dm^{-3}). Scan rates: (a, c) 0.2 V s^{-1}; (b) 0.05 V s^{-1}.

Scheme 3

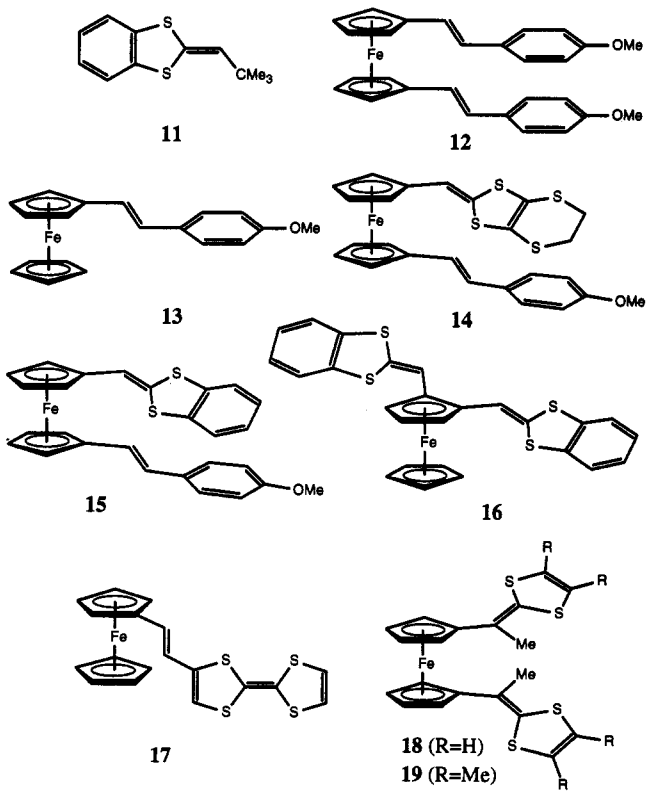

The ability of monoferrocene molecules to undergo stepwise oxidation (neutral/monocation/dication) is generally limited to media of wide anodic window (liquid SO_2[10] or molten salts[11]). To the best of our knowledge, only one other report appeared on highly oxidized ferrocene molecules in common nonaqueous solvents.[12]

Table 1. Formal Electrode Potentials (*vs* SCE) for the Ferrocene-Centered Oxidation Steps Exhibited by the Actual Complexes in Dichloromethane Solution

complex	$E^{\circ\prime}_{0/+}$, V	ΔE_p,[a] mV	$E^{\circ\prime}_{+/2+}$,[b] V	ΔE_p,[b] mV
5	+0.25	84	+0.65	114
6	+0.26	86	+0.77	106
7	+0.36	72		
12	+0.34	98		
13	+0.39	76		
14	+0.29	86	+0.78	110
15	+0.29	86	+0.82	98
16	+0.35	84	+0.86[d]	
1[c]	+0.97	84		
ferrocene	+0.45	88		

[a] Measured at 0.2 V s^{-1}. [b] Measured at 0.5 V s^{-1}. [c] Present work. [d] Peak potential value.

Analysis[13] of the cyclic voltammograms relevant to the first oxidation process with scan rates varying from 0.02 V s^{-1} to 5.12 V s^{-1} shows that (i) the i_{pc}/i_{pa} ratio is constantly equal to 1, (ii) the current function $i_{pa}xv^{-1/2}$ remains essentially constant, and (iii) the peak-to-peak separation progressively increases from 66 to 266 mV. Under the same experimental conditions, the one-electron oxidation of ferrocene displays a rather similar trend of ΔE_p with scan rate, thus indicating that departure from the constant value of 59 mV expected for an electrochemically reversible one-electron transfer[13] should be due to uncompensated solution resistances, rather than to significant structural reorganizations accompanying the charge transfer.[14]

The electrode potentials of the discussed electron removals are compiled in Table 1, together with those of the related complexes presented here.

As shown in Figure 2, complex **5** exhibits a qualitatively similar redox pattern, but the second oxidation process is markedly affected by electrode surface phenomena.

Either the similarity in redox potentials of **5** and **6** or the fact that the solution of $[5]^+$, electrogenerated by controlled potential coulometry (E_w = +0.4 V), even if deep violet in color, also absorbs in the ferrocenium region (γ_{max} = 632 nm; ϵ = 3640 M^{-1} cm^{-1}), both suggest that the substituents of complexes **5** and **6** contribute to the relevant HOMO levels to a similar extent.

With respect to unsubstituted ferrocene and expecially with respect to the 1,1′-ferrocenedicarbaldehyde precursor **1**, it is evident that the present 1,1′-sulfur-based substituents pour a significant amount of electron density on the ferrocene moiety.

As shown in Figure 3, complex **7** displays a somewhat different redox propensity, in that the first reversible anodic process is now followed by a second irreversible step at rather high potential value, which we arbitrarily assign to the substituent-centered oxidation. The dichloromethane solution of $[7]^+$, electrogenerated by controlled potential coulometry (E_w = +0.50 V), is cherry red in color (γ_{max} = 553 nm; ϵ = 3070 M^{-1} cm^{-1}), thus suggesting that here the HOMO level probably receives a lower contribution from the ferrocene fragment.

(10) Sharp, P. R.; Bard, A. J. *Inorg. Chem.* **1983**, *22*, 2689–2693.
(11) Gale, R. J.; Singh, P. *J. Organomet. Chem.* **1980**, *199*, C44–C46.
(12) Moore, A. J.; Skabara, P. J.; Bryce, M. R.; Batsanov, A. S.; Howard, J. A. K.; Daley, S. T. A. K. *J. Chem. Soc., Chem. Commun.* **1993**, 417–419.
(13) Brown, E. R.; Sandifer, J. R. In *Physical Methods of Chemistry. Electrochemical Methods*; Rossiter, B. W., Hamilton, J. F., Eds.; Wiley: New York, 1986; Vol. 2, Chapter 4.
(14) Zanello, P. In *Stereochemistry of Organometallic and Inorganic Compounds*, Bernal, I., Ed.; Elsevier: Amsterdam, 1990; Vol. 4, p 181.

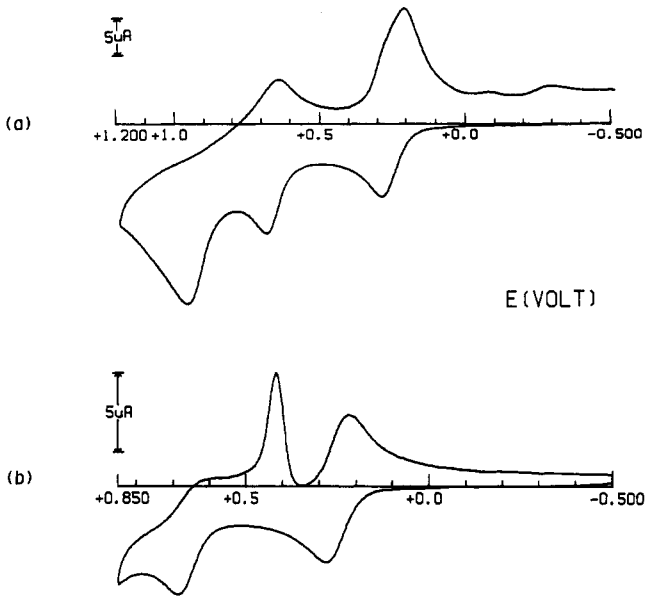

Figure 2. Cyclic voltammograms recorded at a platinum electrode on a CH_2Cl_2 solution containing $[NBu_4][ClO_4]$ (0.2 mol dm^{-3}) and **5** (9.3×10^{-4} mol dm^{-3}). Scan rates: (a) 0.2 V s^{-1}; (b) 0.05 V s^{-1}.

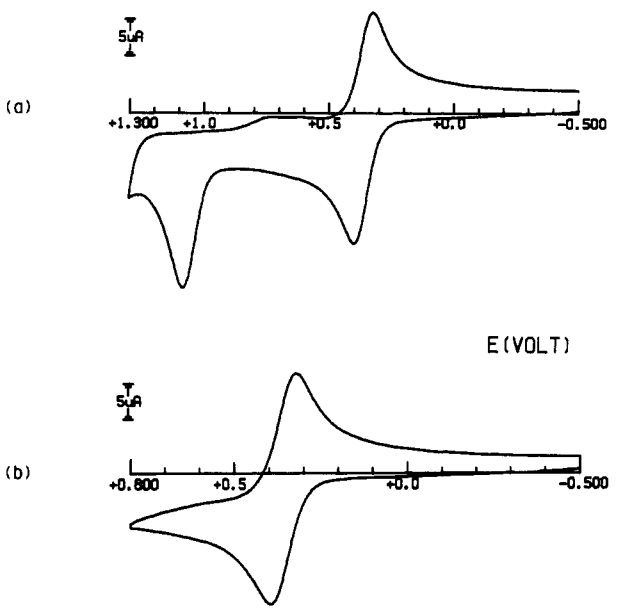

Figure 3. Cyclic voltammetric responses recorded at a platinum electrode on a CH_2Cl_2 solution containing **7** (1.1×10^{-3} mol dm^{-3}) and $[NBu_4][ClO_4]$ (0.2 mol dm^{-3}). Scan rate: 0.2 V s^{-1}.

To better define the electronic factors governing the redox potentials of the present complexes, the related derivatives **12–16** shown in Scheme 3 (see the Experimental Section) have been examined (these compounds react with TCNQ, but no CT complexes could be isolated in a crystalline form). The electron-donating abilities of the 1,1'-substituents are roughly additive, as shown by the first reversible process. In fact, with respect to ferrocene, each $CH{=}CS_2C_6H_4$ or $CH{=}CS_2C_2S_2(CH_2)_2$ substituent makes the electron removal about 95–100 mV easier. On the other hand, a $CH{=}CHC_6H_4$-*p*-OMe group anticipates the oxidation by about 55–60 mV. However, in complex **16** in which the two $CH{=}CS_2C_6H_4$ substituents are attached to the same cyclopentadienyl ring, each group reduces to half its electron-donating ability, probably because of electron-delocalizing effects due to double-bond conjugation.

Table 2. Experimental Data for the X-ray Diffraction Study of 5 and 10

	5	**10**
compound		
formula	$C_{22}H_{18}FeS_8$	$C_{52}H_{34}FeN_8S_2$
mol wt	642.79	890.83
diffractometer	Enraf-Nonius CAD4	Philips PW1100
crystal dim, mm	$0.1 \times 0.1 \times 0.07$	$0.65 \times 0.19 \times 0.05$
data collecn T, °C	23	23
cryst syst	monoclinic	triclinic
space group	$P2_1/c$	$P\bar{1}$
a (Å)	12.488(1)	7.796(1)
b (Å)	12.178(1)	8.607(1)
c (Å)	16.219(1)	16.396(2)
α (deg)		92.88(1)
β (deg)	104.5(1)	97.83(1)
γ (deg)		100.95(1)
V (Å^3)	2387.7(7)	1066.8(5)
Z	4	1
ρ(calcd) (g·cm^{-3})	1.788	1.387
μ (cm^{-1})	13.216	4.919
radiation	Mo Kα (graphite monochromated), γ = 0.710 69 Å	
measured reflcns	$\pm h,+k,+l$	$\pm h,\pm k,+l$
θ range (deg)	2.5–25.0	3.0–25.0
scan type	$\omega/2\theta$	$\omega/2\theta$
scan width (deg)	$1.10 + 0.35 \tan\theta$	$0.8 + 0.35 \tan\theta$
bkgd time (s)	0.5 · scan time	0.5 · scan time
max scan speed (deg · min^{-1})	7.0	1.0 (constant)
prescan rejection limit	0.5 (2.0σ)	
prescan acceptance limit	0.025 (40.0σ)	
no. of indep data coll	4219	3927
no. of obsd reflcns (n_o)	1087	2093
	$\|F_o^2\| > 3.5\sigma(\|F\|^2)$	$\|F_o^2\| > 3.0\sigma(\|F\|^2)$
transm coeff	0.9997–0.8245	
no. of params refined (n_v)	182	286
f	0.06	
R	0.068	0.072
R_w	0.080	0.082
GOF	2.378	2.780

[a] $R = \sum(\|F_o\| - (1/k)|F_c\|)/\sum|F_o|$. [b] $R_w = \sum w(\|F_o\| - (1/k)|F_c\|)^2/[\sum w|F_o|^2]^{1/2}$, where $w = [\sigma^2(F_o)]^{-1}$; $\sigma(F_o) = [\sigma^2(F_o)^2 + f^4(F_o)^2]^{1/2}/2F_o$. [c] GOF $= [\sum w(|F_o| - (1/k)|F_c|^2/(n_o - n_v)]^{1/2}$.

A quite pertinent electrochemical report has recently appeared, dealing with complexes **17–19** (see Scheme 3).[12] These complexes undergo in acetonitrile solution three subsequent anodic steps, similar to the derivatives studied here. In the case of complex **17**, the first oxidation ($E^{\circ\prime}$ = +0.28 V, *vs* SCE) is thought to be centered on the tetrathiafulvalene substituent, whereas for complexes **18** and **19** this first process ($E^{\circ\prime}$ = +0.12 and +0.08 V, respectively) appears to be centered on the interacting ferrocene–dithiole fragment.

Solid-State Structure of Compounds 5 and 10. Relevant parameters concerning the X-ray diffraction studies are collected in Table 2. A view of **5** is depicted in Figure 4, and a selection of bond lengths and angles is given in Table 3, whereas Table 4 collects the final atomic positional parameters. The bond lengths and angles fall in the expected range.[15] We note, however, that the accuracy of the geometrical parameters is somewhat low. This can be judged by the spread in the values of the C–S bond lengths in the range of 1.6–1.9 Å. This is related to the disorder of the terminal C atoms and the high thermal motion of the sulfur atoms (*vide infra*), as well as to the relatively low number of observed reflections.

(15) (a) Orpen, A. G.; Brammer, L.; Allen, F. H.; Kennard, O.; Watson, D. G.; Taylor, R. *J. Chem. Soc., Dalton Trans.* **1989**, Supplement S1-S83. (b) Allen, F. H.; Kennard, O.; Watson, D. G.; Brammer, L.; Orpen, A. G.; Taylor, R. *J. Chem. Soc., Perkin Trans. 2* **1987**, Supplement S1-S19.

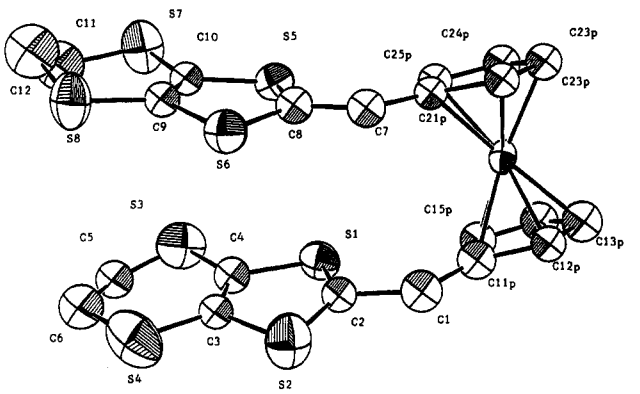

Figure 4. ORTEP drawing and atom numbering scheme of **5** (ellipsoids at the 50% probability level).

Table 3. Selected Interatomic Distances and Angles for 5[a]

	Bond Distances (Å)		
S1–C2	1.67(2)	S6–C9	1.73(2)
S1–C4	1.78(2)	S7–C10	1.75(2)
S2–C2	1.58(2)	S7–C11	1.75(5)
S2–C3	1.77(2)	S8–C9	1.76(2)
S3–C4	1.68(3)	S8–C12	1.82(3)
S3–C5	1.51(3)	C1–C2	1.58(3)
S4–C3	1.72(2)	C1–C11p	1.39(3)
S4–C6	1.83(4)	C3–C4	1.33(3)
S5–C8	1.76(2)	C7–C8	1.39(3)
S5–C10	1.75(2)	C7–C21p	1.44(3)
S6–C8	1.66(2)	C9–C10	1.34(3)
	Bond Angles (deg)		
C2–S1–C4	89.(1)	S4–C3–C4	131.(2)
C2–S2–C3	89.(1)	S1–C4–S3	117.(1)
C4–S3–C5	102.(1)	S1–C4–C3	115.(2)
C3–S4–C6	100.(1)	S3–C4–C3	129.(2)
C8–S5–C10	92.8(9)	C8–C7–C21p	133.(2)
C8–S6–C9	94(1)	S5–C8–S6	117.(1)
C10–S7–C11	99.(2)	S5–C8–C7	120.(1)
C9–S8–C12	100.(1)	S6–C8–C7	123.(1)
C2–C1–C11p	133.(2)	S6–C9–S8	115.(1)
S1–C2–S2	127.(1)	S6–C9–C10	118.(2)
S1–C2–C1	114.(1)	S8–C9–C10	127.(2)
S2–C2–C1	118.(1)	S5–C10–S7	114.(1)
S2–C3–S4	111.(1)	S5–C10–C9	116.(2)
S2–C3–C4	118.(2)	S7–C10–C9	130.(2)

[a] Numbers in parentheses are estimated standard deviations in the least-significant digits.

The most remarkable solid-state feature of this compound is its conformation. The orientation of the two substituents on the ferrocene moiety is such that they lie approximately on top of each other, i.e., the ferrocene unit shows an almost perfectly eclipsed conformation. This is quantitatively expressed by the torsion angles C(1)–C(11p)–C(21p)–C(7) and C(1)–C(2)–C(8)–C(7) of 5(2)° and 0(2)°, respectively. The molecule shows a pseudomirror plane bisecting it and containing the iron atom. This intramolecular overlap is illustrated in Figure 5. Given the eclipsed conformation of the ferrocene moiety, this is not the only limiting molecular symmetry. Indeed, one could imagine that a rigid rotation of 180° around the C(1)–C(11p) axis would lead to a different limiting (chiral) conformation of the molecule having approximate C_2 symmetry. In fact, the latter type of conformation has recently been observed for related derivatives bearing conjugated substituents.[12,16] To our knowledge, the conformation observed for compound **5** is unprecedented and may be due to the significant attractive interaction between the two sulfur-containing fragments, but this remains to be proven. However, the two sulfur heterocycles are not parallel, but they are found to (1) diverge, as indicated by the increasing separation between corresponding couples of sulfur atoms in the upper and lower rings, varying from 3.69 to 4.58 Å, for S(1)–S(5)/S(2)–S(6) and S(4)–S(8)/S(3)–S(7), respectively, and (2) to be rotated out of the plane of the respective Cp rings. This distortion is reflected by the angles between the couples of planes defined by the Cp's and those of the heterocyclic five-membered rings (21° in both cases). Obviously, such a distorsion, if still present also in the CT complex **8**, will be detrimental as far as intermolecular interaction of the ferrocene components is concerned.

Another aspect worth noting concerns the disorder of both terminal CH_2CH_2 groups. As can be seen in Figure

(16) Gelin, F.; Thummel, R. P. *J. Org. Chem.* **1992**, *57*, 3780–3783.

Table 4. Final Positional Parameters and Equivalent Temperature Factors for 5[a]

atom	*x*	*y*	*z*	B_{eq},[b] Å²
Fe	0.1665(3)	0.2901(3)	–0.1784(2)	2.97(7)
S1	0.1826(5)	0.4209(6)	0.0641(4)	4.5(2)
S2	0.4133(6)	0.3847(7)	0.1520(5)	6.6(2)
S3	0.1576(6)	0.6199(7)	0.1610(5)	6.6(2)
S4	0.4364(6)	0.5727(9)	0.2626(6)	8.1(3)
S5	0.1684(5)	0.6549(6)	–0.0826(4)	4.2(2)
S6	0.4051(5)	0.6491(6)	–0.0004(4)	4.8(2)
S7	0.1271(6)	0.8710(7)	–0.0155(5)	6.5(2)
S8	0.4128(6)	0.8657(7)	0.0820(5)	6.4(2)
C1	0.311(2)	0.268(2)	0.012(2)	5.2(6)*
C2	0.307(2)	0.364(2)	0.077(1)	2.6(5)*
C3	0.347(2)	0.501(2)	0.183(1)	2.7(4)*
C4	0.241(2)	0.519(2)	0.144(1)	4.1(6)*
C5	0.223(2)	0.667(2)	0.245(2)	2.2(6)*
C6	0.345(3)	0.683(3)	0.280(2)	4.6(9)*
C7	0.310(2)	0.505(2)	–0.122(1)	4.0(5)*
C8	0.300(1)	0.596(2)	–0.073(1)	1.7(4)*
C9	0.332(2)	0.764(2)	0.017(1)	3.6(5)*
C10	0.223(2)	0.767(2)	–0.019(1)	3.4(5)*
C11	0.199(4)	0.936(5)	0.078(3)	8(2)*
C12	0.313(2)	0.978(3)	0.067(2)	8.5(9)*
C11p	0.234(2)	0.226(2)	–0.058(1)	4.3(6)*
C12p	0.250(2)	0.156(2)	–0.126(1)	3.5(5)*
C13p	0.151(2)	0.126(2)	–0.176(2)	4.8(6)*
C14p	0.064(2)	0.172(2)	–0.146(1)	4.6(6)*
C15p	0.113(2)	0.235(2)	–0.079(1)	4.1(6)*
C21p	0.231(2)	0.443(2)	–0.185(1)	3.0(5)*
C22p	0.259(2)	0.369(2)	–0.245(1)	3.4(5)*
C23p	0.161(2)	0.333(2)	–0.300(1)	3.8(5)*
C24p	0.070(2)	0.381(2)	–0.275(1)	4.2(6)*
C25p	0.110(2)	0.450(2)	–0.206(1)	3.5(5)*
C5a	0.270(6)	0.724(7)	0.228(5)	2(2)*
C6a	0.316(5)	0.630(6)	0.308(4)	3(2)*
C11a	0.213(4)	0.977(4)	0.048(3)	3(1)*

[a] Esd's on the last significant digit are given in parentheses. [b] Starred values denote atoms refined isotropically. Anisotropically refined atoms are given in the form of the isotropic equivalent displacement parameter defined as $B_{eq} = {}^4/_3[a^2B(1,1) + b^2B(2,2) + c^2B(3,3) + ab(\cos\gamma)B(1,2) + ac(\cos\beta)B(1,3) + bc(\cos\alpha)B(2,3)]$.

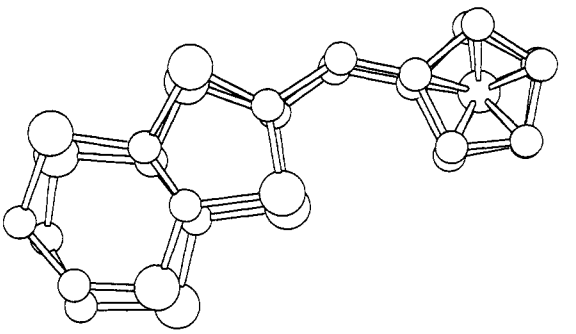

Figure 5. Illustration of the eclipsed conformation ("intramolecular stacking") of **5** in the solid state.

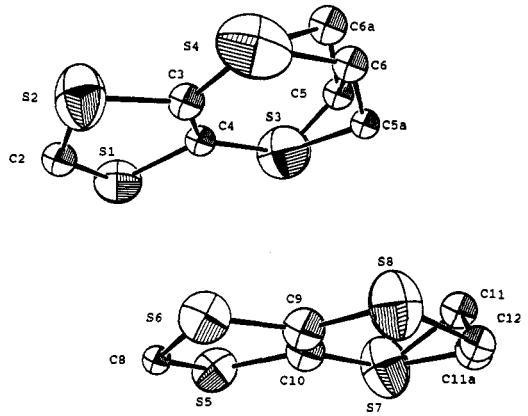

Figure 6. The different conformations and the disorder in the substituents of **5**.

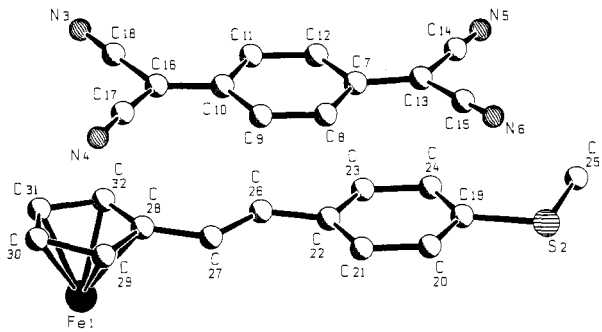

Figure 7. Schakal plot of the asymmetric unit of **10** and atom numbering scheme.

6, the two six-membered rings adopt different conformations. For the ring containing S(3) and S(4), there are three possible conformations, the major one being best described as a twisted boat (occupancy ca. 0.7). The other two possibilities account for the rest of the occupancy and correspond to approximate boat conformations. The observed connectivity is consistent with the deformation leading from one boat conformation to the opposite one. In the other ring (containing S(7) and S(8)), the disorder is less resolved, the observed conformations being twisted (occupancy ca. 0.7) and an approximate boat. Similar disorder features have been observed for several BEDT-TTF derivatives.[17]

A view of the asymmetric unit of **10** is provided by Figure 7 (atom numbering scheme), and a selection of bond distances and angles is given in Table 5, whereas Table 6 provides atomic positional parameters. The iron atom coincides with a crystallographic inversion center. This leads to a perfect antiperiplanar arrangement of the two substituents attached to the ferrocene core. The TCNQ molecules are placed one above and one below each of the (methylthio)phenyl substituents. Thus, along the shortest crystallographic axis *a*, corresponding to the longest macroscopic crystal dimension, there is an alternation of acceptor and donor molecules. A projection along this axis is depicted in Figure 8, whereas Figure 9 provides a view along the *b* axis. Such an arrangement explains the insulator nature of this compound.

The shape and size of the donor and the acceptor in this CT complex fit particularly well with one another. The phenyl rings of the symmetry-related substituents are nearly coplanar with the Cp rings, the angle between these planes being 4°. Parallelism is observed between the Cp and the six-membered ring of TCNQ (interplane angle = 2.3°). The distance between the planes of the TCNQ molecules and of the aromatic substituent are, within one standard deviation, equal to the distance between the Cp rings in the ferrocene fragment (3.32 Å). Furthermore, the intermolecular Fe–Fe distances, because of the crystallographic symmetry, correspond to the unit cell constants. A further relatively short Fe–Fe separation of 10.46

(17) For a discussion, see: Williams, J. M.; Wang, H. H.; Emge, T. J.; Geiser, U.; Beno, M. A.; Leung, P. C. W.; Carlson, K. D.; Thorn, R. J.; Schultz, A. J. *Progr. Inorg. Chem.* **1987**, *35*, 51–218.

Table 5. Selected Interatomic Distances[a] and Angles[a] for 10

	Bond Distances (Å)		
S2–C19	1.77(2)	C10–C11	1.44(2)
S2–C25	1.79(2)	C10–C16	1.37(2)
N3–C18	1.13(2)	C11–C12	1.36(2)
N4–C17	1.16(2)	C13–C14	1.47(2)
N5–C14	1.16(2)	C13–C15	1.41(2)
N6–C15	1.11(2)	C16–C17	1.41(2)
C7–C8	1.43(2)	C16–C18	1.42(2)
C7–C12	1.42(2)	C22–C26	1.43(2)
C7–C13	1.36(2)	C26–C27	1.33(2)
C8–C9	1.34(2)	C27–C28	1.45(2)
C9–C10	1.42(2)		
	Bond Angles (deg)		
C19–S2–C25	99.7(8)	C10–C16–C18	125.(1)
C7–C13–C14	124.(1)	C17–C16–C18	111.(1)
C7–C13–C15	123.(1)	N4–C17–C16	176.(2)
C14–C13–C15	112.(1)	N3–C18–C16	179.(2)
N5–C14–C13	174.(1)	C22–C26–C27	130.(2)
N6–C15–C13	174.(2)	C26–C27–C28	129.(2)
C10–C16–C17	123.(1)		

[a] Numbers in parentheses are estimated standard deviations in the least-significant digits.

Table 6. Final Positional Parameters and Equivalent Temperature Factors for 10[a]

atom	*x*	*y*	*z*	B_{eq},[b] Å^2
Fe1	0.0000	0.5000	0.0000	3.20(8)
S2	0.1464(8)	−0.2756(7)	−0.4269(4)	10.9(2)
N3	−0.658(1)	0.093(1)	−0.0266(7)	5.3(4)
N4	−0.641(2)	0.417(1)	−0.2151(9)	7.2(5)
N5	−0.287(2)	−0.540(1)	−0.3250(8)	7.2(4)
N6	−0.343(2)	−0.229(2)	−0.5240(9)	8.2(5)
C7	−0.409(2)	−0.164(1)	−0.3234(8)	2.9(4)
C8	−0.436(2)	−0.014(2)	−0.3516(9)	3.8(4)
C9	−0.488(2)	0.089(2)	−0.3006(8)	3.6(4)
C10	−0.519(2)	0.048(1)	−0.2199(8)	2.7(4)
C11	−0.488(2)	−0.100(1)	−0.1886(9)	3.7(4)
C12	−0.435(2)	−0.201(1)	−0.2417(8)	3.2(4)
C13	−0.363(2)	−0.273(2)	−0.3745(9)	4.7(4)
C14	−0.326(2)	−0.426(2)	−0.350(1)	5.2(5)
C15	−0.345(2)	−0.250(2)	−0.4579(9)	4.4(4)
C16	−0.579(2)	0.150(1)	−0.1692(8)	3.7(4)
C17	−0.616(2)	0.297(2)	−0.193(1)	5.1(5)
C18	−0.624(2)	0.118(2)	−0.0900(9)	4.4(4)
C19	0.085(2)	−0.176(1)	−0.3413(8)	3.4(4)
C20	0.059(2)	−0.027(2)	−0.363(1)	6.0(5)
C21	0.010(2)	0.076(2)	−0.3055(9)	4.2(4)
C22	−0.015(2)	0.026(1)	−0.2286(8)	3.2(4)
C23	0.016(2)	−0.121(2)	−0.2079(9)	4.8(5)
C24	0.065(2)	−0.226(2)	−0.2642(9)	4.8(4)
C25	0.162(2)	−0.462(2)	−0.385(1)	9.1(6)
C26	−0.069(2)	0.106(2)	−0.161(1)	7.8(6)
C27	−0.094(2)	0.254(2)	−0.151(1)	5.6(5)
C28	−0.156(2)	0.329(2)	−0.826(9)	4.1(4)
C29	−0.194(2)	0.484(2)	−0.102(1)	6.0(5)
C30	−0.260(2)	0.540(1)	−0.0284(8)	4.4(4)
C31	−0.239(2)	0.426(2)	0.031(1)	6.6(5)
C32	−0.186(2)	0.296(2)	−0.005(1)	6.1(5)

[a] Esd's on the last significant digit are given in parentheses. [b] Atoms were refined isotropically. Anisotropically refined atoms are given in the form of the isotropic equivalent displacement parameter defined as $B_{eq} = {}^4/_3[a^2B(1,1) + b^2B(2,2) + c^2B(3,3) + ab(\cos\gamma)B(1,2) + ac(\cos\beta)B(1,3) + bc(\cos\alpha)B(2,3)]$.

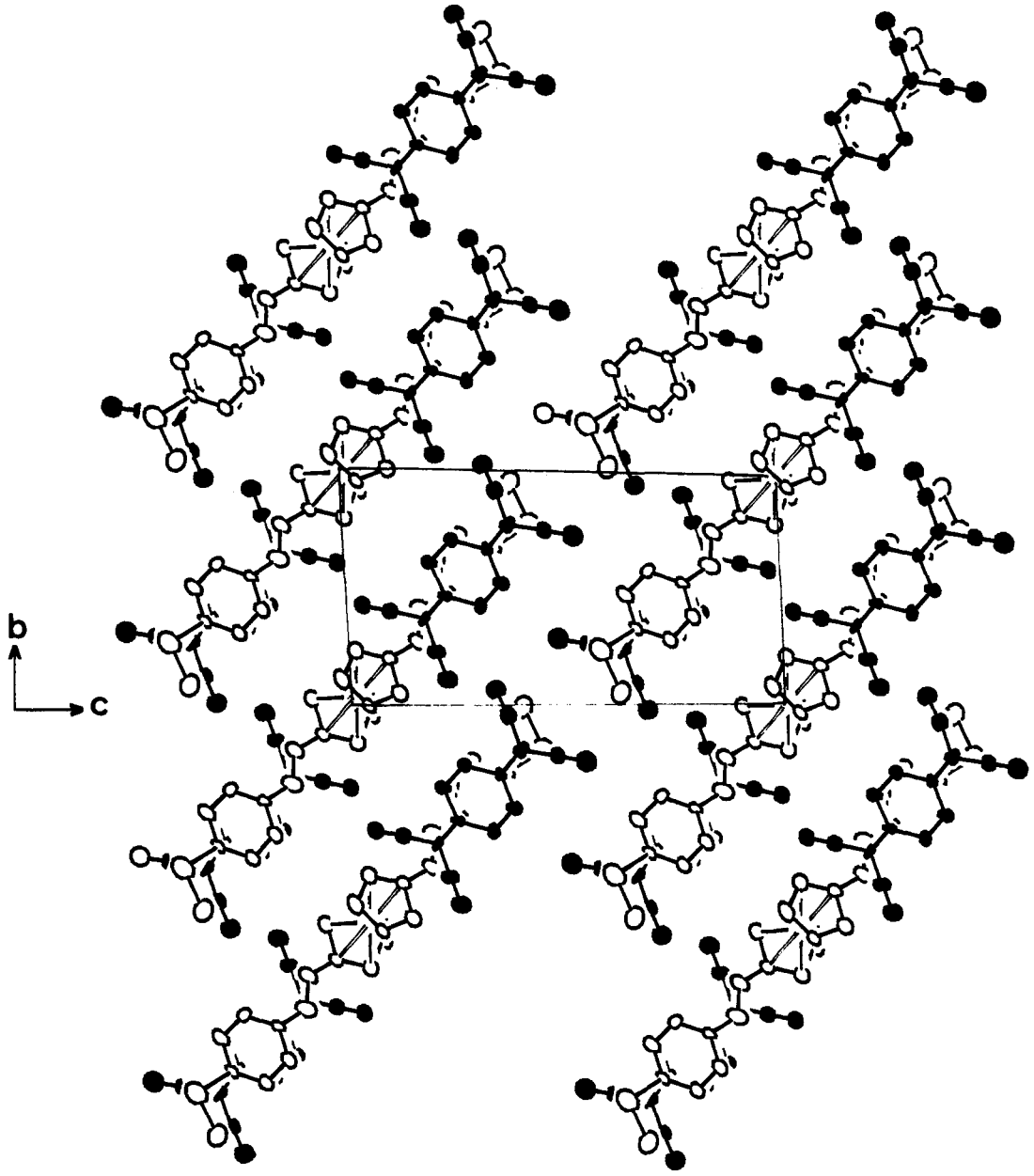

Figure 8. Packing diagram of **10** projected along the *a* axis. Atoms in TCNQ molecules are represented by filled ellipsoids.

Å is found along the diagonal of the *ab* plane. Such distances (7.80, 8.61, and 10.46 Å) are in part shorter than those found in, e.g., the ferromagnetic CT complex $[FeCp^*2]^+[TCNE]^-$,[4] where the shortest distance between iron atoms is 8.73 Å.

Magnetic Measurements. Magnetic susceptibility measurements were carried out for the CT complexes **8–10**. The temperature dependence of χ^{-1} and χT for compounds **8** and **9** (which both exibit a similar magnetic behavior over the entire temperature range investigated), corrected for a weak background signal, is displayed in Figure 10. As shown in Figure 10a, the temperature dependence of χ for these two compounds at high temperatures ($T \geq 50$ K) is well described by the simple Curie–Weiss law, $\chi = C/(T-\theta)$, with $\theta = -3(2)$ K and $\theta = -4(2)$ K, respectively. The negative sign of θ suggests that antiferromagnetic interactions could dominate the magnetic behavior below 50 K, giving rise to antiferromagnetic order in these compounds at very low temperatures. The likely occurence of antiferomagnetic coupling between the electronic magnetic moments is also seen in Figure 10b, where the quantity χT, a measure of the effective magnetic moment, is plotted as a function of temperature. The effective moments, calculated from $\mu_{eff} = (3\chi k_B/NT)^{1/2}$ from the high-temperature data, are $1.89\mu_B$ and $1.97\mu_B$ for **8** and **9**, respectively. As the samples of **8** and **9** are cooled below 50 K, an abrupt drop in χT is observed, indicating the approach of a phase transition possibly dominated by antiferromagnetic interactions to a magnetically ordered state, with a critical temperature (Néel temperature) of $T_N < 5$ K. However, although similar results were previously reported for other ferrocene-containing CT complexes,[18] the observed behavior could also be explained by a depopulation of spin-orbit states, and not by a magnetic ordering.

In contrast to compounds **8** and **9**, no significant

(18) See, e.g.: (a) Miller, J. S.; Ward, M. D.; Zhang, J. H.; Reiff, W. M. *Inorg. Chem.* **1990**, *29*, 4063–4072. (b) Miller, J. S.; Calabrese, J. C.; Rommelmann, H.; Chittipeddi, S. R.; Zhang, J. H.; Reiff, W. M.; Epstein, A. J. *J. Am. Chem. Soc.* **1987**, *109*, 769–781. (c) Heuer, W. B.; Mountford, P.; Green, M. L. H.; Bott, S. G.; O'Hare, D.; Miller, J. S. *Chem. Mater.* **1990**, *2*, 764–772.

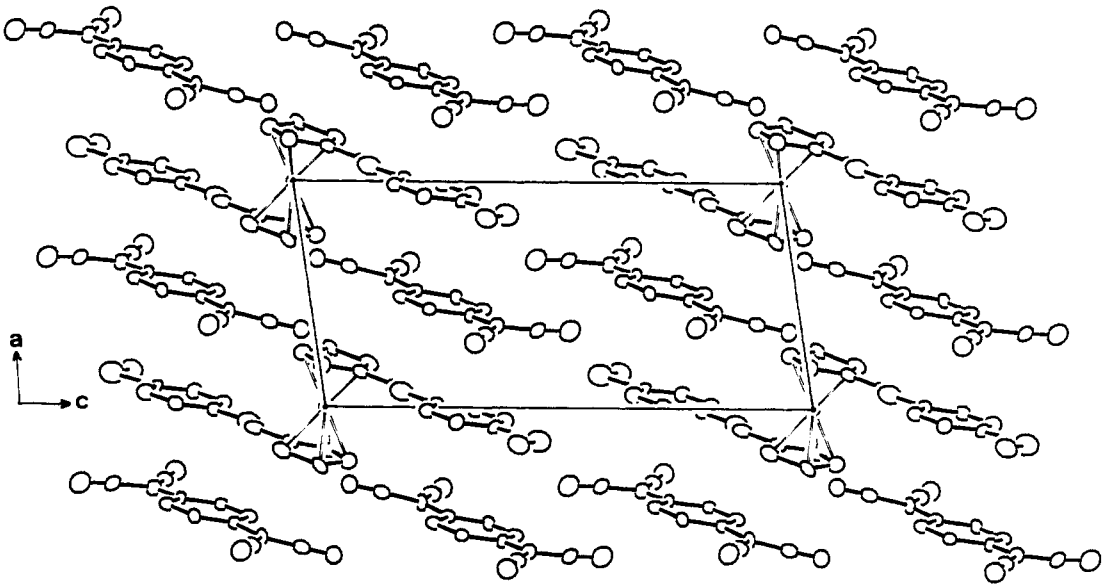

Figure 9. Packing diagram of **10** projected along the *b* axis.

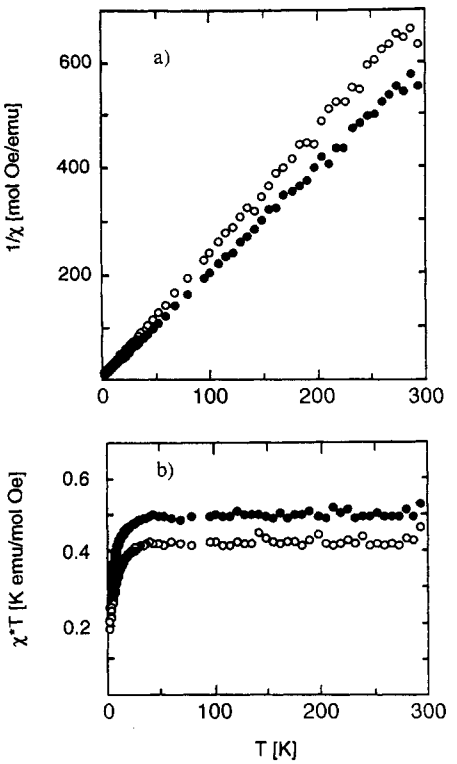

Figure 10. Temperature dependence of the magnetic susceptibility (a) χ^{-1} and (b) χT for compound **8** (open circles) and **9** (solid circles) measured in an external magnetic field of 500 Oe.

magnetic signal above the noise level could be observed for the CT complex **10**.

ESR Spectroscopy. The two compounds **8** and **9** exhibit a very similar behavior. At room temperature a symmetric line shape is observed, which is compatible with electron transfer between donor and acceptor. It could in principle also be due to a delocalization of the electron hole from the iron into the sulfur heterocycle. It should, however, be pointed out that due to a different relaxation times not all species of unpaired electrons contributing to the paramagnetic susceptibility are necessarily observed in the ESR spectrum. It is very well possible that the electrons in the weakly conducting aromatic stacks are not observed in the experiments described here. They contribute, however, to the observed susceptibility.

The *g* values at 294 K are $g(8) = 2.005$ and $g(9) = 1.995$. As the temperature is lowered, the resonances broaden (see Figure 11), and at very low temperature the ESR spectra are typical for a nearly axial Fe^{3+} complex, with the following *g* values: $g_{\parallel}(9) = 2.893$, $g_{\parallel}(8) = 2.577$, $g_{\perp}(9) = 2.048$, $g_{\perp}(8) = 2.016$ (low-temperature *g* values measured at 5 K).

According to susceptibility measurements, within the Curie approximation, one obtains at 5 K for **8** $g^2S(S + 1) = 1.84$, and for **9**, $g^2S(S + 1) = 1.80$. Assuming a spin $S = {}^1/_2$ at the iron site and an isotropic *g* value of 2.33, one obtains 40% of (isolated) paramagnetic iron ions for **9** and about the same value for **8**. This deviation from 100% is very probably due to antiferromagnetic coupling between the electron spins on the irons. These values show that the CT complex is formed primarily between the iron ions and the TCNQ molecules and not between the heterocyclic substituents and TCNQ. Unfortunately the temperature dependence of the conductivity is not yet available, and no correlation of this temperature dependence with the ESR parameters can be carried out at present.

The ESR susceptibility (χ) of the two compounds was measured between room temperature and 5 K. The qualitative behavior of the ESR susceptibilities as a function of temperature is the same for both compounds. Below 200 K, along with the emerging of the Fe^{3+} powder pattern, χT remains constant down to ca. 30 K. In this region the paramagnetic iron ions exhibit a Curie type behavior. Below 30 K the decrease of χT is indicative of an antiferromagnetic coupling between the electron spins on the irons. These results are in good agreement with those obtained from magnetic susceptibility measurements (vide supra).

A motion-averaged resonance is observed for CT complex **10** at all temperatures with an indication of a slight *g* anisotropy at low temperature. The ESR intensity for this compound is extremely weak, thus indicating a very low degree of charge transfer. The two experimental *g* values for **10** are $g(294\ K) = 2.003$ and $g(5\ K) = 2.002$. Because of the low degree of charge transfer, the observed decrease of χT with decreasing temperature is reflecting a back-transfer of unpaired electrons, thus reducing the

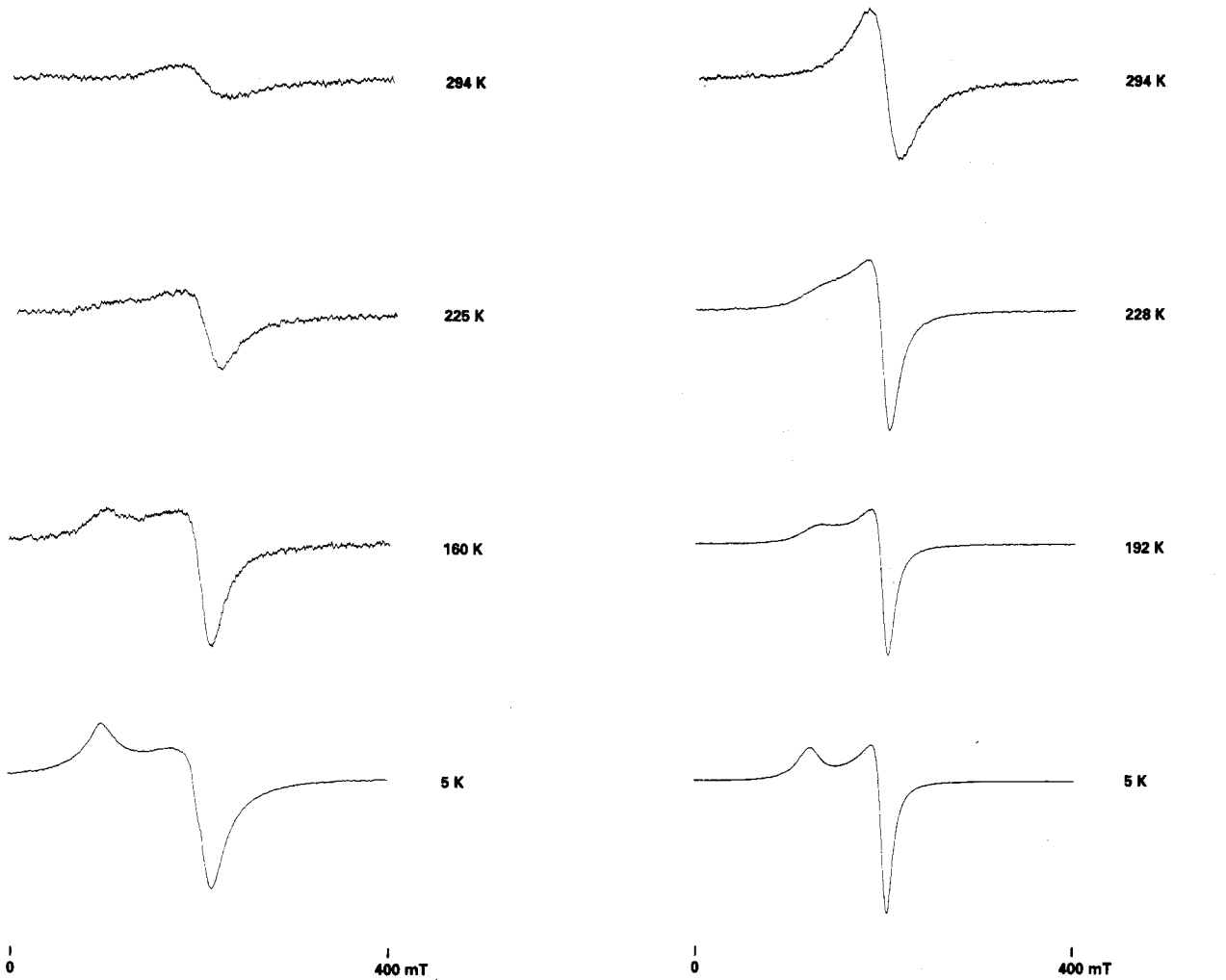

Figure 11. Temperature dependence of the ESR spectra for samples of **8** (a, left and **9** (b, right).

concentration of CT ion pairs. This indicates that the system tends, at very low temperature, to a diamagnetic ground state.

Conclusions

We have shown that suited substitution in the 1,1′-position of the ferrocene core affords electron donors which can preferentially assume an eclipsed conformation in the solid state. This is the case for compound **5** and very likely also for its analog **6**. This feature leads to a structural situation which is characterized by what can be called "intramolecular stacking". Such an arrangement is thought to favor the formation of segregated stacks of donors and acceptors, thus leading to conducting materials, as has been shown for the CT complexes **8** and **9**. On the other hand, when the donor assumes a preferred antiperiplanar conformation, as in **7**, the corresponding CT complex **10** turns out to be an insulator by virtue of the alternance of donor and acceptor moieties in the solid state. Furthermore, the combination of different donor fragments within the same molecule affords systems from which one or two electrons can be reversibly removed, although it is not yet clear whether or not the dicationic state of **5** and **6** can be realized in the form of a CT complex. Because of the relatively high degree of conformational freedom still present in these molecules, their geometry cannot yet be considered to constitute an optimum. In order to circumvent this drawback, further synthetic manipulations are currently underway with the aim of preparing donors containing the same basic molecular components, but which are more rigid and more symmetric.

Experimental Section

General Considerations. Synthesis. All reactions with air- or moisture-sensitive materials were carried out under Ar using standard Schlenk techniques. Freshly distilled, dry, and oxygen-free solvents were used throughout. Routine ^{1}H NMR spectra (250.133 MHz) were recorded with a Bruker AC 250 spectrometer. Chemical shifts are given in ppm relative to internal TMS, and coupling constants (J) are given in hertz. Low-resolution EI/MS spectra were recorded at 70 eV on a Finnigan MAT 212/SS300 spectrometer. Merck silica gel 60 (70–230 mesh) was used for column chromatography. Thin-layer chromatography (TLC) was performed with Merck silica gel 60 F254 precoated glass plates. Infrared spectra were recorded with a Perkin-Elmer 1720 IR FT spectrometer on Nujol mulls. Elemental analyses were performed by Analytical Research Services, CIBA-GEIGY AG.

1,1′-Bis[(5,6-dihydro-1,3-dithiolo[4,5-*b*][1,4]dithiin-2-ylidene)methyl]ferrocene (5). 2-(Dimethoxyphosphoryl)-5,6-dihydro-1,3-dithiolo[4,5-*b*][1,4]dithiin, **2**[7] (756 mg, 2.5 mmol) was dissolved in 25 mL of THF and cooled to −78 °C. Then 1.8 mL (2.9 mmol) of 1.6 M BuLi in hexane was added, and the solution was stirred for 15 min, after which 303 mg (1.25 mmol) of 1,1′-ferrocenedicarbaldehyde (**1**)[6] dissolved in 8 mL of THF was added dropwise. The red reaction mixture was stirred for 1 h at −78 °C and allowed to warm to room temperature and stirred overnight. The brick-red suspension was filtered, giving a first crop of microcrystalline product. The mother liquor was

concentrated, and the residue was chromatographed on a plug of silica gel, using CH_2Cl_2 as eluent. The combined fractions of crude product were recrystallized from hot 1,2-dichloroethane. Yield: 530 mg of bordeaux-red crystals (71%). ^1H NMR: δ 3.26 (s, 8H), 4.12 (t, J = 1.5, 4H), 4.25 (t, J = 1.5, 4H), 5.90 (s, 2H). MS: m/z 594 (M^+), 566, 536, 472, 446, 402, 386, 312, 298, 296, 222, 150 (100). Anal. Calcd for $C_{22}H_{18}FeS_8$: C, 44.43; H, 3.05; S, 43.13. Found: C, 44.62; H, 3.24; S, 42.53.

1,1'-Bis[(1,3-benzodithiol-2-ylidene)methyl]ferrocene (6). This compound was prepared in a similar manner as described above, starting from 2.05 g (7.8 mmol) of 2-(dimethoxyphosphoryl)-1,3-benzodithiole (**3**)[8] and 5.63 mL (9.0 mmol) of 1.6 M BuLi in hexane, in 60 mL of THF, and 940 mg (3.9 mmol) of **1** dissolved in 20 mL of THF. The brick-red crystalline product was purified by recrystallization from hot EtOH (or alternatively from ethyl acetate by addition of hexane). Yield: 1.505 g (75%). ^1H NMR: δ 4.17 (t, J = 1.5, 4H), 4.36 (t, J = 1.5, 4H), 5.98 (s, 2H), 6.90–7.12 (complex m, 8H). MS: m/z 514 (M^+, 100), 285, 257, 229, 197, 152. Anal. Calcd for $C_{26}H_{18}FeS_4$: C, 60.69; H, 3.53; S, 24.93. Found: C, 60.46; H, 3.60; S, 24.83.

1,1'-Bis[2-[4-(methylthio)phenyl]-(*E*)-ethenyl]ferrocene (7). To a solution of 7.0 g (20.9 mmol) of [4-(methylthio)-benzyl]triethylphosphonium bromide (**4**, prepared from commercially available 4-(methylthio)benzyl alcohol, via bromination with PBr_3 and pyridine, followed by reation with PEt_3 in refluxing benzene) in 40 mL of MTBE was added a solution of 20.1 mL (32.16 mmol) of 1.6 M BuLi in 40 mL of MTBE, and the mixture was stirred first at 0 °C for 0.5 h and then for 1 h at room temperature. A suspension of 2.53 g (10.45 mmol) of **1** in 20 mL of MTBE was added to the orange solution of the Wittig reagent, and the mixture was stirred for 2 days. The resulting orange-red suspension was filtered, giving 2.77 g of crude solid material, which proved by NMR to be the title compound, contaminated with LiBr. This was washed with ether and dissolved in CH_2Cl_2, and the solution was washed with H_2O. Drying over $MgSO_4$, evaporation of the solvent and recrystallization from hot cyclohexane afforded 2.31 g (46%) of pure **7**. ^1H NMR: δ 2.45 (s, 6H), 4.18 (t, J = 1.5, 4H), 4.35 (t, J = 1.5, 4H), 6.04 (AB q, J = 13.8, 4H), 7.08 (AA'BB' system, 8H). MS: m/z 482 (M^+, 100), 434, 269, 254, 241, 210, 165. Anal. Calcd for $C_{28}H_{26}FeS_2$: C, 69.70; H, 5.43. Found: C, 69.70; H, 5.80. The mother liquor contained a ca. 1:1 mixture (by NMR) of **7** and its *Z*/*E*-isomer. Attempted separation by flash column chromatography proved difficult and did not give satisfactory results.

Preparation of Charge-Transfer Complexes. The procedure for the preparation of CT complexes is exemplified by compound **8**. A 149-mg (0.25-mmol) sample of **5** and 102 mg (0.50 mmol) of TCNQ (purchased from Fluka and used without further purification) were dissolved in equal amounts of 1,2-dichloroethane (15 mL), the solutions were heated to reflux temperature, and traces of insoluble material were filtered off. The solution of the ferrocene derivative was then added to that of TCNQ and the resulting dark brown mixture briefly stirred. Slow cooling to room temperature led to the formation of very thin, black needles. These were filtered off, washed with small portions of 1,2-dichloroethane, and dried in vacuo. Yield: 158 mg (63%). Anal. Calcd for $C_{46}H_{26}FeN_8S_8$: C, 55.08; H, 2.61; N, 11.17; S, 25.57. Found: C, 55.13; H, 2.67; N, 11.25; S, 25.20.

Compound **9** was obtained in an analogous manner from 129 mg (0.25 mmol) of **6** and 102 mg (0.50 mmol) of TCNQ in 30 mL of 1,2-dichloroethane. Yield: 188 mg (81%). Anal. Calcd for $C_{50}H_{26}FeN_8S_4$: C, 65.07; H, 2.84; N, 12.14; S, 13.90. Found: C, 65.32; H, 2.96; N, 12.24; S, 13.92.

Compound **10** was prepared from 500 mg (1.04 mmol) of **7** and 424.7 mg (2.08 mmol) of TCNQ in 105 mL of 1,2-dichloroethane. Yield: 770 mg (86%). Anal. Calcd for $C_{52}H_{34}FeN_8S_2$: C, 70.11; H, 3.85; N, 12.58; S, 7.20. Found: C, 70.40; H, 4.10; N, 12.70; S, 7.10.

Synthesis of Model Systems. Compound **11** was prepared in 65% yield from reagent **3** and pivalaldehyde under the conditions used for the preparation of **6**. ^1H NMR: δ 1.19 (s, 9H), 5.53 (s, 1H), 7.0–7.05 (m, 2H), 7.11–7.17 (m, 2H).

Compound **12** was prepared similarly to **7** in 45% yield. ^1H NMR: δ 3.76 (s, 6H), 4.17 (t, J = 1.5, 4H), 4.33 (t, J = 1.5, 4H), 6.53 (br s, 4H), 6.71–7.15 (AA'BB' system, 8H). MS: m/z 450 (M^+, 100), 253, 240, 225. Anal. Calcd for $C_{28}H_{26}FeO_2$: C, 74.78, H, 5.82. Found: C, 74.59; H, 5.90.

Compound **13** was prepared from formylferrocene by a procedure analogous to the one used for **12** in 55% yield. ^1H NMR: δ 3.77 (s, 3H), 4.07 (s, 5H), 4.19 (t, J = 1.5, 2H), 4.38 (t, J = 1.5, 2H), 6.62 (AB system, J = 16, 2H), 6.80–7.30 (AA'BB' system, 4H).

Compounds **14** and **15** were prepared from **1** by stepwise addition of the Wittig reagent generated form [*p*-$MeOC_6H_4CH_2$-PPH_3]Cl upon deprotonation with MeOLi in MeOH/DMF, followed by either **2** or **3**. **14**: 35% overall yield. ^1H NMR: δ 3.45 (s, 4H), 4.00 (s, 3H), 4.35 (br t, J = 1.5, 2H), 4.39 (br t, J = 1.5, 2H), 4.45 (br t, J = 1.5, 2H), 4.59 (br t, J = 1.5, 2H), 6.18 (s, 1H), 6.80 (br s, 2H), 7.05–7.54 (AA'BB' system, 4H). MS: m/z 522 (M^+, 100), 494, 374, 297, 253, 238. Anal. Calcd for $C_{25}H_{22}FeOS_4$: C, 57.46; H, 4.24; S, 24.54; Fe, 10.69. Found: C, 57.45; H, 4.31; S, 23.92; Fe, 11.0. **15**: 39% overall yield. ^1H NMR: δ 3.76 (s, 3H), 4.17 (br t, J = 1.5, 2H), 4.21 (br t, J = 1.5, 2H), 4.34 (br t, J = 1.5, 2H), 4.38 (br t, J = 1.5, 2H), 6.00 (s, 1H), 6.60 (m, AB system, 2H), 6.70 (high-field part of AA'BB' system, 2H), 6.97 (m, 4H), 7.20–7.28 (m, 2H). MS: m/z 482 (M^+, 100), 253, 238. Anal. Calcd for $C_{27}H_{22}FeOS_2$: C, 67.22; H, 4.60; S, 13.29. Found: C, 67.10; H, 4.63; S, 13.20.

Compound **16** was prepared analogously to **6** starting from 1,2-diformylferrocene[19] in 58% yield. ^1H NMR: δ 4.23 (s, 5H), 4.46 (br t, J = 1.5, 1H), 4.78 (d, J = 1.5, 2H), 6.29 (s, 2H), 7.10–7.19 (m, 4H), 7.21–7.35 (m, 4H). MS: m/z 514 (M^+, 100), 378, 285, 253. Anal. Calcd for $C_{26}H_{18}FeS_4$: C, 60.69; H, 3.53; S, 24.93. Found: C, 60.54; H, 3.63; S, 24.60.

Physical Measurements. Electrochemistry. Anhydrous dichloromethane (packaged under nitrogen, 100-mL bottles, Aldrich) for electrochemistry and tetrabutylammonium perchlorate supporting electrolyte (dried and stored in a vacuum oven at 40 °C, Fluka) were commercial products. The cyclic voltammetric measurements were performed with a BAS 100A electrochemical analyzer. A three-electrode cell was designed to allow the tip of the saturated calomel electrode (SCE) to approach closely, via a Luggin capillary, the platinum disk working electrode, which in turn was surrounded by a platinum spiral counter electrode. Controlled potential coulometry was carried out by using a AMEL-Mod. 552 potentiostat, connected to an AMEL-Mod. 558 integrator. A three-compartment cell was designed with a central unit bearing a platinum gauze working macroelectrode. The lateral compartments contained the reference (SCE) and the auxiliary (mercury pool) electrodes, respectively. The compartments containing the working and the auxiliary electrodes were separated by a sintered-glass disk. In situ visible spectra of products electrogenerated by macroelectrolysis were recorded with a Lambda 2 Fiber Optic System UV/vis spectrometer (Perkin-Elmer). Deoxygenation of the solutions was achieved by bubbling ultrapure nitrogen for at least 10 min. All of the potential values are referred to SCE.

Crystallography. Structural Sturdy of 5. Deep red crystals of compound **5** were obtained by crystallization from ethyl acetate and are stable in the air. A prismatic crystal was chosen for the data collection and was mounted on a glass fiber in a random orientation. An Enraf-Nonius CAD4 diffractometer was used both for the unit cell and space group determination and for the data collection. Unit-cell dimensions were obtained by least-square fit of the 2θ values of 25 high-order reflections ($9.41 < \theta < 18.75°$), using the CAD4 centering routine. Selected crystallographic and other experimental data are listed in Table 2.

Data were measured with variable scan speed to ensure constant statistical precision on the collected intensities. Three standard reflections were used to check the stability of the crystal

(19) For the synthesis of 1,2-$Fc(CHO)_2$ see, e.g.: Goldberg, S. I.; Bailey, W. D. *J. Am. Chem. Soc.* **1974**, *96*, 6381–6387.

and of the experimental conditions and were measured every hour. The orientation of the crystal was checked by measuring three other reflections every 300 measurements. Data have been corrected for Lorentz and polarization factors using the data reduction programs of the MOLEN crystallographic package.[20] An empirical absorption correction[21] was applied by using azimuthal (ψ) scans of two "high-χ-angle" reflections ($\chi > 87°$). The standard deviations on intensities were calculated in terms of statistics alone, while those on F_o were calculated as reported in Table 2. Intensities were considered as observed if $|F_o^2| > 3.5\sigma(F^2)$ and used for the solution and refinement of the structure. The structure was solved by Patterson and Fourier methods and refined by full-matrix least squares. The function minimized was $[\sum(w|F_o| - 1/k|F_c|)^2]$. No extinction correction was applied. Other relevant parameters for the refinement are listed in Table 2. The scattering factors used, corrected for the real and imaginary parts of the anomalous dispersion, were taken from the literature.[22] Anisotropic displacement parameters were used for all atoms, except those disordered (i.e., C5, C6, C11, C12). The contribution of the hydrogen atoms in their idealized positions (C–H = 0.95 Å) was taken into account but not refined. Upon convergence no parameter shift was $> 0.4\sigma(p)$. All calculations were carried out by using the MOLEN crystallographic programs.[20] The final atomic coordinates and isotropic equivalent displacement parameters are given in Table 4.

Structural Study of 10. It proved impossible to find untwined crystals of **10**. Eventually, a small needle-shaped crystal (grown from hot 1,2-dichloroethane) was found in which the angular separation of the reflections belonging to the two individuals was sufficiently wide to allow the indexing and the collection of the intensities belonging to one of the two individuals. A Philips PW1100 diffractometer was used for the cell constant determination (using 25 high-angle reflections) and for the data collection. A constant scan speed was used: other relevant crystallographic and experimental data are given in Table 2. Given the small size of the crystal and the low absorption coefficient, no correction for absorption was necessary. The structure was solved and refined as described above, using anisotropic displacement parameters for all non-hydrogen atoms. The final atomic coordinates and isotropic displacement parameters are given in Table 6.

Conductivity. Samples of the CT complexes (ca. 80–100 mg) were pressed to pellets, and room temperature conductivity was measured by the standard four-probe method.

Magnetic Measurements. The magnetic susceptibility χ of compounds **8–10** was measured in the temperature range of 2–300 K in an external magnetic field of 500 Oe by means of a *Quantum Design* superconducting quantum interference device (SQUID) magnetometer. The polycrystalline samples were mounted in a sample holder tube made of quartz glass in order to keep the magnetic background a low as possible.

ESR Spectra. ESR experiments were performed on a Varian E9 ESR spectrometer equipped with an Oxford Instruments continuous-flow cryostat ESR 910 and a temperature controller ITC4.

Acknowledgment. M.H. is grateful to the Swiss National Science Fundation for financial support (grant 21-36220.92) and A.T. thanks Mr. Robert Häusel (CIBA-GEIGY Ltd.) for preparative work.

Supplementary Material Available: Tables of bond distances and angles, torsion angles, anisotropic displacement parameters, and calculated positional parameters for hydrogen atoms for **5** and **10** (20 pages). Ordering information is given on any current masthead page.

OM930741R

(20) *MOLEN: Molecular Structure Solution Procedure*; Enraf Nonius: Delft, The Netherlands, 1990.

(21) North, A. C. T.; Phillips, D. C.; Mathews, F. S. *Acta Crystallogr. Sect. A* **1968**, *A24*, 351.

(22) *International Tables for X-Ray Crystallography*; Kynoch Press: Birmingham, UK, 1974; Vol. IV.